WATER RESOURCES RESEARCH, VOL. 37, NO. 11, PAGES 2687–2698, NOVEMBER 2001

Extended tailing of bacteria following breakthrough at the Narrow Channel focus area, Oyster, Virginia

Pengfei Zhang,[1,2] William P. Johnson,[1] Timothy D. Scheibe,[3] Keun-Hyung Choi,[4] Fred C. Dobbs,[4] and Brian J. Mailloux[5]

Abstract. Extended tailing of low bacterial concentrations following breakthrough at the Narrow Channel focus area was observed for 4 months. Bacterial attachment and detachment kinetics associated with breakthrough and extended tailing were determined by fitting a one-dimensional transport model to the field breakthrough-tailing data. Spatial variations in attachment rate coefficient (k_f) were observed under forced gradient conditions (i.e., k_f decreased as travel distance increased), possibly because of decreased bacterial adhesion with increased transport distance. When pore water velocity decreased by an order of magnitude at 9 days following injection, apparent bacterial attachment rate coefficients did not decrease with velocity as expected from filtration theory, but, instead, increased greatly for most of the wells. The coincidence of the increase in apparent attachment rate coefficient with the occurrence of protist blooms suggested that the loss of bacteria from the aqueous phase during the protist blooms was not governed by filtration but rather was governed by predation. Simulations were performed to examine the transport distances achieved with and without detachment, using attachment and detachment rate coefficients similar to those obtained in this field study. Simulations that included detachment showed that transport distances of bacteria may significantly increase because of detachment under the conditions examined.

1. Introduction

Bacterial transport in the subsurface is influenced by advection, hydrodynamic dispersion, attachment, and detachment, as well as by other factors including growth, death, starvation, motility, chemotaxis, and predation [*Peterson and Ward*, 1989; *Murphy and Ginn*, 2000]. Particular interest in microbial detachment arises from its potential importance on microbial transport. Persistent low concentrations of microbes in the aqueous phase resulting from detachment may pose significant risk to drinking water safety if the microbes are pathogenic. Detachment may also slowly redistribute the microbial mass downgradient, significantly increasing the distances of microbial transport over large timescales.

Persistent low concentrations of microbes following breakthrough (hereafter referred to as extended tailing) indicative of detachment have been observed in many laboratory column experiments [*Fontes et al*., 1991; *Hornberger et al*., 1992; *Lindqvist et al*., 1994; *McCaulou et al*., 1994, 1995; *Johnson et al*., 1995; *Hendry et al*., 1997, 1999; *Harter et al*., 2000]. In addition, various means of simulating detachment kinetics have been included in transport models to simulate some of these results [*Hornberger et al*., 1992; *McCaulou et al*., 1994, 1995; *Johnson et al*., 1995; *Hendry et al*., 1997, 1999]. Extended tailing of microbial concentrations has been observed in several field-scale transport experiments [*Scholl and Harvey*, 1992; *Harvey et al*., 1995; *Ryan et al*., 1999; *DeBorde et al*., 1999; *Schijven et al*., 1999]. However, among those field transport studies, only two have monitored the extended tailing over long periods of time (months) [*Harvey et al*., 1995; *Schijven et al*., 1999], and only one has modeled the kinetics of attachment and detachment [*Schijven et al*., 1999]. Therefore information regarding the attachment and detachment kinetics of long-term microbial transport in the field is rare, and the significance of detachment on field microbial transport over large timescales is not well understood.

The dependence of bacterial attachment rate on transport distance is an important consideration in field-scale microbial transport. It has been recently recognized that distributions in bacterial attachment efficiencies exist even within a monoclonal population [*Albinger et al*., 1994; *Simoni et al*., 1998; *Baygents et al*., 1998; *Glynn et al*., 1998; *Bolster et al*., 1999, 2000]. A distribution of attachment efficiencies within the bacterial population can be expected to result in attachment rates that decrease with transport distance [*Bolster et al*., 1999, 2000], and attachment rates determined at small scales (e.g., column scale) can be expected to underestimate transport at larger scales (e.g., field scales) [*Bolster et al*., 1999; 2000]. Decreased attachment rate with increased transport distance has been observed for protozoa [*Harvey et al*., 1995] and viruses [*Schijven et al*., 1999]. *Hendry et al*. [1997] found that irreversible bacterial attachment rate coefficients decreased with increasing transport distances (3.5–40 cm) in quartz sand column experiments.

The relationship between the attachment rate and pore wa-

[1]Department of Geology and Geophysics, University of Utah, Salt Lake City, Utah, USA.
[2]Now at Department of Earth and Environmental Science, New Mexico Institute of Mining and Technology, Socorro, New Mexico, USA.
[3]Pacific Northwest National Laboratories, Richland, Washington, USA.
[4]Department of Ocean, Earth and Atmospheric Sciences, Old Dominion University, Norfolk, Virginia, USA.
[5]Department of Geosciences, Princeton University, Princeton, New Jersey, USA.

Paper number 2000WR000151.
0043-1397/01/2000WR000151$09.00

ter velocity has been investigated in laboratory column experiments [*Wollum and Cassel*, 1978; *Smith et al*., 1985; *Tan et al*., 1994; *Hendry et al*., 1999]. Results from these column experiments show that bacterial breakthrough concentrations increase with increasing pore water velocity. Numerical simulations indicate that the attachment rate coefficients increased with increasing velocity for some strains [*Tan et al*., 1994; *Hendry et al*., 1999], whereas the attachment rate coefficient was independent of velocity for a highly hydrophobic strain [*Hendry et al*., 1999]. Studies by *Tan et al*. [1994] and *Hendry et al*. [1999] have indicated that bacterial detachment rate coefficients were independent of pore water velocity under the conditions of the experiments. The relationship between attachment and detachment rates and pore water velocity under field conditions, however, has not been well documented.

The objectives of this study were (1) to monitor the long-term extended tailing of bacteria during field transport and to determine the rates of bacterial attachment and detachment associated with bacterial breakthrough and extended tailing, (2) to examine the dependence of bacterial attachment rates on transport distances achieved in the field, (3) to examine the effects of pore water velocity change on bacterial attachment and detachment rates in the field, and (4) to determine the significance of detachment on transport distances over large timescales.

2. Methods

To achieve the above objectives, bacterial breakthrough and extended tailing were monitored over a 4-month period in the field. Bacterial attachment and detachment rate coefficients were determined by fitting a one-dimensional (1-D) bacterial transport model to the field data. The attachment rate coefficients determined from breakthrough data at different sampling points were compared and related to transport distance. Cessation of groundwater extraction 9 days following injection caused an order of magnitude decrease in pore water velocity during the experiment, and the attachment and detachment rate coefficients (for a given well) at the two different velocities were compared to examine the effects of velocity on the attachment and detachment kinetics. Transport simulations with and without detachment were performed to evaluate the significance of detachment on transport distances.

2.1. Experimental Setup

2.1.1. Site description. The Oyster Site is located on the Delmarva Peninsula near the town of Oyster, Virginia, and the Narrow Channel focus area is located in the oxic region of the Oyster Site (Figure 1). A silt loam layer at ~7-m depth below mean sea level (msl) serves as a lower boundary of the surficial aquifer at the Narrow Channel focus area. The sediments composing the surficial aquifer at this area include quartz, feldspar, clays, and Fe and Al hydroxides in decreasing order of abundance (H. J. Dong et al., Transport of adhesion deficient bacteria in heterogeneous porous media: Relative dominance of physical versus chemical control on bacterial transport, submitted to *Environmental Science Technology*, 2001) (hereinafter referred to as Dong et al., submitted manuscript, 2001). The fine-grained quartz and feldspars are typically coated with clays (illite/smectite) and metal hydroxides, while the coarse quartz and feldspars are relatively depleted in metal oxide coatings (Dong et al., submitted manuscript, 2001). Aquifer sediment grain sizes range from 177 to 707 μm with a

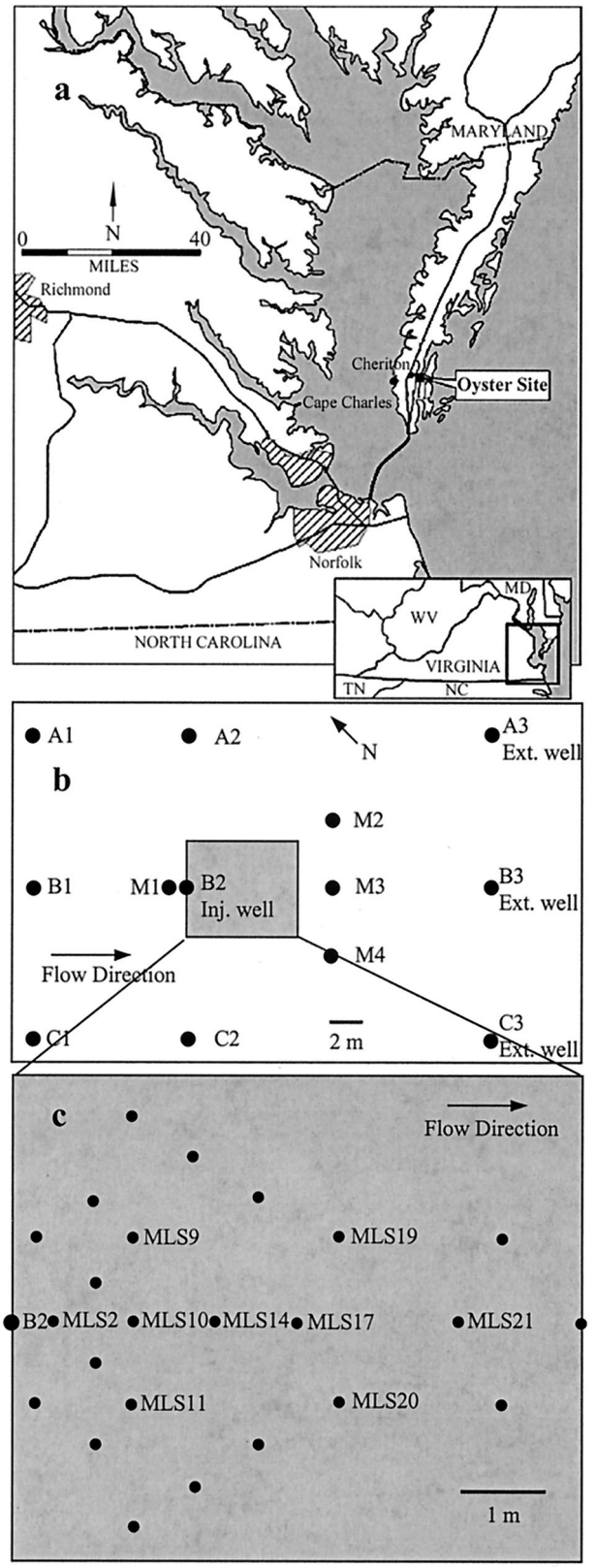

Figure 1. (a) Site location, (b) flow cell configuration, and (c) multilevel sampler layout for the Narrow Channel focus area. B2 is the injection well, and A3, B3, and C3 are the extraction wells. Bacterial samples from port 9 at MLS 2, 9, 10, 11, 14, 17, 19, 20, and 21 were examined in this study. Figure 1a is from *Scheibe et al.* [2001]. (Reprinted from *Ground Water* with permission of the National Ground Water Association. Copyright 2001.)

mean value of 354 μm, and porosity of the aquifer varies from 0.25 to 0.4 with a mean value of 0.3.

The flow cell in the Narrow Channel focus area comprises an array of 24 multilevel samplers (MLSs) located immediately downgradient from an injection well B2 (Figure 1). Each MLS has 12 sampling ports evenly spaced between the depths of 3 and 6 m below msl. Details of the design and installation of the MLSs are described by *Johnson et al*. [2001a] and *Scheibe et al*. [2001]. Three extraction wells A3, B3, and C3, which were screened over the lower 6 m of the surficial aquifer, were installed on the downgradient end of the flow cell and were used to set up a steady state flow field across the cell (Figure 1).

Hydraulic conductivity data indicated that a relatively high permeability zone existed at a depth of ~4.5–5 m below msl (corresponding to ports 8 and 9) at all locations in the flow cell, except at the location of MLS 10, where the flow axis showed relatively low permeability, i.e., surrounding the location of MLS 10 [*Hubbard et al*., 2001; *Johnson et al*., 2001a]. Groundwater chemistry and grain size were relatively constant across the flow cell in the high-permeability zone (port 8 and 9). For example, pH ranged from 5.6 to 5.9, ionic strength ranged from 3.0 to 3.5 m*M*, total organic carbon ranged from 0.4 to 0.6 ppm, and grain size ranged from 177 to 500 μm (B. J. Mailloux et al., The role of heterogeneity on the field-scale transport and attachment of bacteria, submitted to *Water Resources Research*, 2001) (hereinafter referred to as Mailloux et al., submitted manuscript, 2001).

2.1.2. Bacterial strain and tracking methods. *Comamonas* DA001, an indigenous bacterial strain isolated from the Oyster Site, was used in this field transport study. An adhesion-deficient variant of DA001 (1.1 μm long by 0.3 μm wide, with a density of approximately 1.06 g cm^{-3}) was developed by a simple column assay [*DeFlaun et al*., 1990] using Oyster Site sediment. The inoculum was grown and stained with the vital fluorescent stain carboxyfluorescein diacetate succinimidyl ester [*DeFlaun et al*., 2001; *Fuller et al*., 2000, 2001]. About 800 L of bacterial suspension (1.36×10^8 cells mL^{-1} in Narrow Channel groundwater) were prepared for the field injection. Bacterial cell counts in this study were determined by flow cytometry (Mailloux et al., submitted manuscript, 2001) for the samples collected during the first week of the experiment and by ferrographic tracking [*Johnson et al*., 2001a] for the remaining samples. Ferrographic tracking combines the selectivity of immunomagnetic separation (IMS) with the resolution of capture cytometry. After sample collection, IMS technique is used to tether magnetic beads (50 nm) to the bacteria of interest. Capture cytometry is then performed using a Bio-Ferrograph instrument to deposit the magnetically tagged bacteria onto an exceedingly small area on a glass surface. The bacteria are then enumerated under an epifluorescence microscope.

The potential influence of motility and metabolic activity on bacterial transport was avoided in this study by using a nonmotile bacterial strain that was starved prior to field injection. The influence of chemotaxis on bacterial transport during this field experiment was expected to be insignificant, because of lack of motility and the relatively constant water chemistry in the high-permeability zone across the site. Previously published field data [*Johnson et al*., 2001a] indicate that cell growth, cell lysis, and stain loss were not significant during the first 9 days of the experiment, as indicated by agreement among growth-based, stain-based, and stable isotope–based bacterial tracking techniques applied to the field samples collected during this period. There are also indications that cell growth, cell lysis, and stain loss were slight at later times (months following injection). For example, per-cell fluorescence by flow cytometric analyses of field samples collected over the 4-month period of the study remained constant [*Fuller et al*., 2001], indicating that little cell growth and stain loss occurred during transport. Laboratory studies examining cell counts in field samples that were refrigerated at 4°C following collection showed constant cell counts (determined by ferrographic tracking) over the course of a month-long holding period [*Johnson et al*., 2001b], indicating a lack of significant cell lysis, cell growth, and stain loss under these conditions.

Monitoring of protist populations (overwhelmingly flagellates) was performed by filtering up to 30 mL of groundwater samples onto Poretic polycarbonate black filters (0.8 μm pore size and 25-mm diameter, Osmonics Inc., Livermore, California) followed by staining with 4′6′-diamidino-2-phenylindole (DAPI) and enumeration by epifluorescence microscopy.

2.1.3. Field experiment protocol. Prior to injection, a forced hydraulic gradient (corresponding to a pore water velocity of ~1 m d^{-1}) was established by pumping at the extraction wells A3, B3, and C3 at rates of 10.41, 41.64, and 20.82 L min^{-1}, respectively. DA001 and bromide (85 mg L^{-1}) were coinjected at a rate of 1 L min^{-1} into B2 over a half-meter interval centered at a depth of 5.0 m below msl, corresponding to the vertical interval between ports 8 and 9 in the high-permeability zone. The injection zone was isolated with packers, and extracted site groundwater was injected simultaneously at 4 L min^{-1} above the isolated zone to maintain an overall injection rate of 5 L min^{-1} at B2. No injection occurred below the isolated zone (below port 9). The injection started on October 29, 1999, at 1735 LT and lasted for 12 hours. The extraction wells were shut down on November 7, 1999, at 1615 LT (9 days following initiation of injection), after which time the hydraulic gradient of the flow cell relaxed to its natural value (corresponding to a pore water velocity of about 0.1 m d^{-1}). Intensive sampling was conducted in ports 5 through 12 at all the MLSs during the first week of the experiment. Sampling of port 9 in select MLSs (MLS 2, MLS 9, MLS 11, MLS 14, MLS 19, MLS 20, and MLS 21) continued for 4 months after the shutdown of the extraction wells to determine the long-term extended tailing of the injected bacteria. Bacterial samples were preserved with 1% formaldehyde and stored at 4°C prior to analysis. Further details of the field experimental protocol are given by *Johnson et al*. [2001a] and *Scheibe et al*. [2001].

2.2. Modeling Bacterial Transport

2.2.1. Governing equations. Microbial transport in porous media was modeled using an advection-dispersion equation that included microbial attachment to and detachment from the porous media. The transport model for a one-dimensional flow system was expressed as

$$\frac{\partial C}{\partial t} = D\,\frac{\partial^2 C}{\partial x^2} - v\,\frac{\partial C}{\partial x} - R_A + R_D \tag{1}$$

$$\frac{\rho_b}{\theta}\,\frac{\partial S}{\partial t} = R_A - R_D, \tag{2}$$

where C is the microbial concentration in aqueous phase (cells per unit volume of water), S is the microbial concentration on solid phase (cells per unit mass of sediment), t is the travel time, ρ_b is the sediment bulk density, θ is the porosity, D is the

hydrodynamic dispersion coefficient, v is the travel velocity, x is the travel distance, R_A is the rate of attachment of microbes to the solid phase, and R_D is the rate of detachment of microbes from the solid phase.

A relatively simple transport model that was capable of capturing the various morphological features of the bacterial breakthrough-elution curve was used to quantify the microbial attachment and detachment rate coefficients, since the goal of this analysis was to examine the effect of changes in scale and pore water velocity on these parameters. Microbial attachment and detachment were modeled as first order reactions and described as

$$R_A = k_f C \tag{3}$$

$$R_D = \frac{\rho_b}{\theta} k_r S_r, \tag{4}$$

where k_f and k_r are the attachment and detachment rate coefficients, respectively, and S_r is the microbial concentration on solid phase that is reversibly attached (i.e., detachable).

Given the inherent heterogeneity of the subsurface, as well as variations in surface properties within bacterial cultures, the rate coefficients determined from the experimental data represent average values across the transport distance to the sampling port. Since the goal of this investigation was to examine trends in the rate coefficients with changes in scale and velocity, the use of average rate coefficient values is acceptable but with the recognition that actual rate coefficients at particular locations across the transport distance would likely vary around the average value.

The order of magnitude velocity decrease in response to cessation of extraction at 9 days provided an opportunity to compare the observed changes in rates of microbial attachment (k_f) in response to the velocity decrease to changes that would be expected based on filtration theory [*Harvey and Garabedian*, 1991]:

$$k_f = \frac{3(1-\theta)}{2d} \alpha \eta v, \tag{5}$$

where d is the effective grain diameter, α is the collision efficiency, and η is the single-collector efficiency. The single-collector efficiency η is the ratio of the rate at which particles strike the collector to the rate at which particles flow toward the collector. The collision efficiency α describes the fraction of collisions with the collector that result in attachment. The single-collector efficiency reflects the measured physical properties of the porous media and the particles, whereas the collision efficiency reflects the chemistry and unmeasured physical properties of the system. In this paper, the single-collector efficiency was estimated as follows [*Rajagopalan and Tien*, 1976; *Rajagopalan et al*., 1982; *Tien*, 1989; *Logan et al*., 1995]:

$$\eta = 4.0 A_S^{1/3} N_{\mathrm{Pe}}^{-2/3} + A_S N_{\mathrm{LO}}^{1/8} N_R^{15/8} + 3.38 \times 10^{-3} A_S N_G^{1.2} N_R^{-0.4}, \tag{6}$$

where A_S is the Happel correction factor, N_{Pe} is the Peclet number, N_{LO} is the London–van der Waals attraction number, N_R is the interception number, and N_G is the gravitation number. Detailed descriptions of A_S, N_{Pe}, N_{LO}, and N_R are given by *Logan et al*. [1995] and *Ryan and Elimelech* [1996]. *Martin et al*. [1996] concluded that for grain-size mixtures the appropriate grain-size measure to use in the filtration equations is d_{10} (the tenth percentile of the grain-size distribution). Therefore a d_{10} value of 200 μm was used in calculations involving filtration theory.

2.2.2. Particle model. A one-dimensional discrete random walk particle model was used to simulate the transport of bromide and bacteria (equations (1) and (2)). Random walk models are a well-known alternative to continuum models for simulating transport in porous media [e.g., *Ahlstrom et al*., 1977; *Prickett et al*., 1981; *Tompson and Gelhar*, 1990; *Kinzelbach and Uffink*, 1991]. Random walk models have advantages of being computationally efficient for large problems, globally mass conservative, flexible, and intuitive. However, simulation of reactive transport is challenging because of the need to convert between particle number and concentration at each time step in order to evaluate reactions written in terms of concentrations. In the particle model used here, standard approaches for simulating advection and dispersion were employed [*Ahlstrom et al*., 1977]. To avoid errors in converting between particle number and concentration, the first-order attachment and detachment rates were represented directly using probabilities of attachment or detachment as follows. The probability of attachment (or detachment) in any time step was given by the attachment (or detachment) rate coefficient multiplied by the time step. At each time step and for each particle a uniform pseudorandom number on the interval [0, 1] was drawn and compared to the attachment (or detachment) probability. If the pseudorandom number was less than the imposed probability, then the particle attached (or detached). To represent the microbial concentration on solid phase that was reversibly attached (S_r), a new parameter, faction of irreversibility (f_{ir}), was introduced. A pseudorandom number was generated upon each occurrence of particle attachment and compared to f_{ir}. If the random number was less than f_{ir}, the particle became permanently attached. For application to bacterial transport the particle model is attractive because of its ability to represent complex processes not easily incorporated into continuum models such as time-dependent irreversibility, variable attachment rates within bacterial populations, and exclusion of colloid-size particles from low-velocity regions of the pore space. The particle model was validated by comparison of results for several simple cases with analytical solutions as encoded in the CXTFIT transport model [*Toride et al*., 1995].

2.2.3. Parameter estimation and sensitivity analysis. Characteristics of the field bacterial breakthrough-elution curve are illustrated in Figure 2. Under forced gradient conditions (prior to 9 days, shaded areas in Figure 2) the field bacterial transport data included breakthrough, elution, and tailing (the latter was referred to as forced gradient tailing) (see Figure 2a).

Under natural gradient conditions the data showed a steep slope from 9 to ~20 days (herein referred to as steep natural gradient tailing) and a shallow slope afterward (herein referred to as shallow natural gradient tailing) (see Figure 2b).

Model parameters that needed to be estimated were v, α_L (longitudinal dispersivity), k_f, k_r, and f_{ir}. The order of magnitude decrease in pore water velocity at 9 days from ~1 m d^{-1} (forced gradient) to 0.1 m d^{-1} (natural gradient) required two separate bacterial transport simulations to be performed for the two different pore water velocities. The simulated aqueous and sediment phase bacterial concentrations at the end of forced gradient were used as initial conditions for the simulation of the bacterial transport data under natural gradient

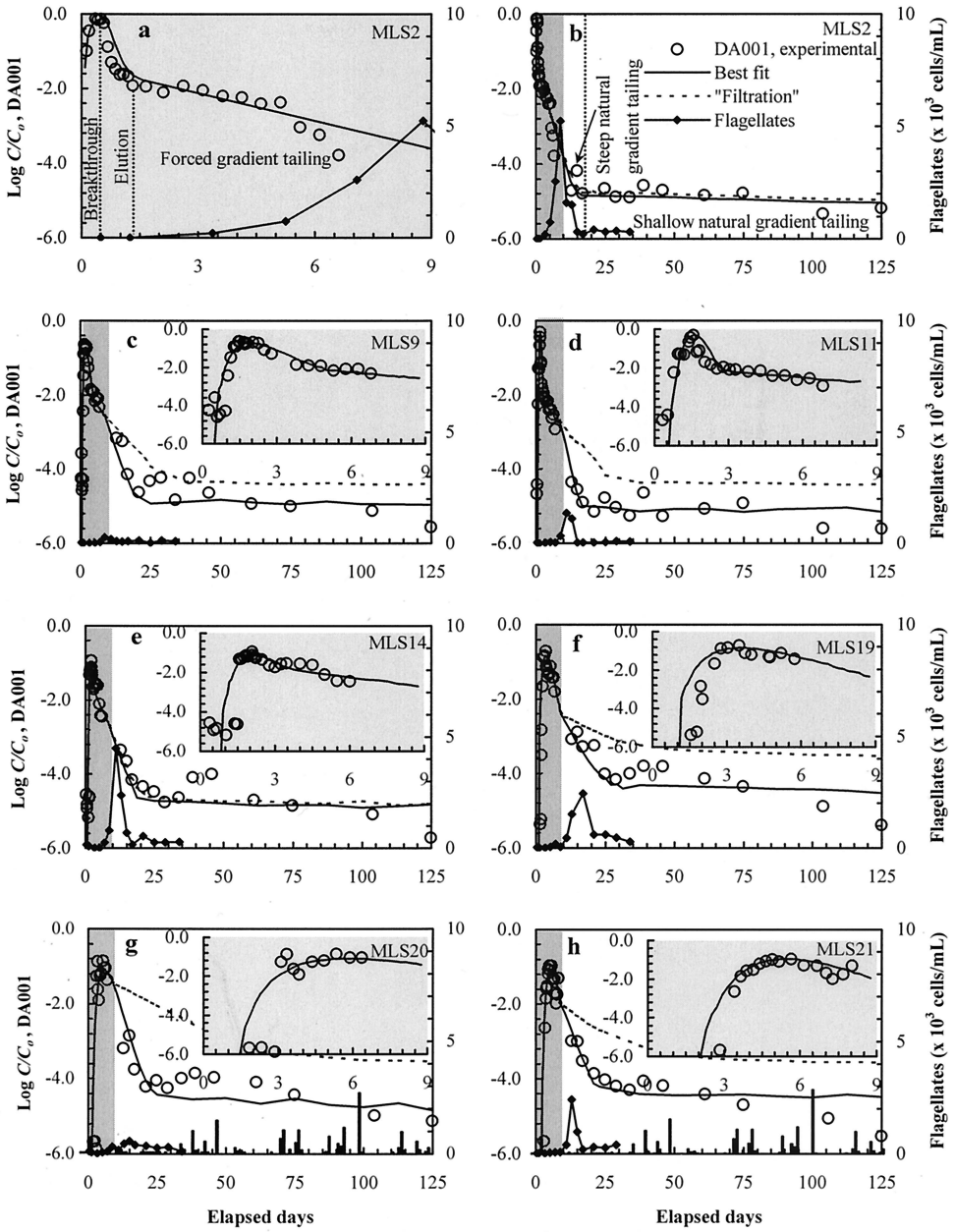

Figure 2. Field bacterial breakthrough-tailing data from port 9 (circles) at selected multilevel samplers (MLSs) with simulations (smooth curves): (a) MLS 2, (b) MLS 2, (c) MLS 9, (d) MLS 11, (e) MLS 14, (f) MLS 19, (g) MLS 20, and (h) MLS 21. Bacterial concentrations were normalized to the initial concentration (C_0, 1.36×10^8 cells mL^{-1}) at the injection well. The smooth solid curves represent the best fit simulations, whereas the smooth dashed curves represent the prediction from filtration theory (see text for explanation). The diamonds represent the flagellate abundance, and the bars in Figures 2g and 2h represent the amount of rainfall (maximum rainfall around 98 days corresponding to 3.0 cm). The forced gradient conditions (shaded area) shown for 9 days in Figure 2a are represented in Figures 2b–2h, which have a much longer time course.

conditions. Since two simulations in series were required, nonlinear regression could not be applied to bacterial simulations to derive the model parameters. Hence best visual fit of the particle model to the field bacterial breakthrough-tailing data was performed to derive the model parameters. Efficiencies of fit (E) [*Hornberger et al.*, 1992] were determined from data excluding flow cytometry values below $C/C_0 = 10^{-5}$ (~1000 cells mL^{-1}), since this is the quantitation limit of that method [*Johnson et al.*, 2001a]. A parameter estimation protocol was developed (see sections 2.2.3.1 and 2.2.3.2) to ensure that the best visual fit was unique.

2.2.3.1. Forced gradient conditions: Velocity (v) and dispersivity (α_L) under forced gradient conditions were derived by inverse modeling of the field bromide breakthrough data using the particle transport model in conjunction with UCODE, an inverse model framework that performs parameter estimation using nonlinear regression [*Poeter and Hill*, 1998]. In bromide simulations the values of k_f, k_r, and f_{ir} were

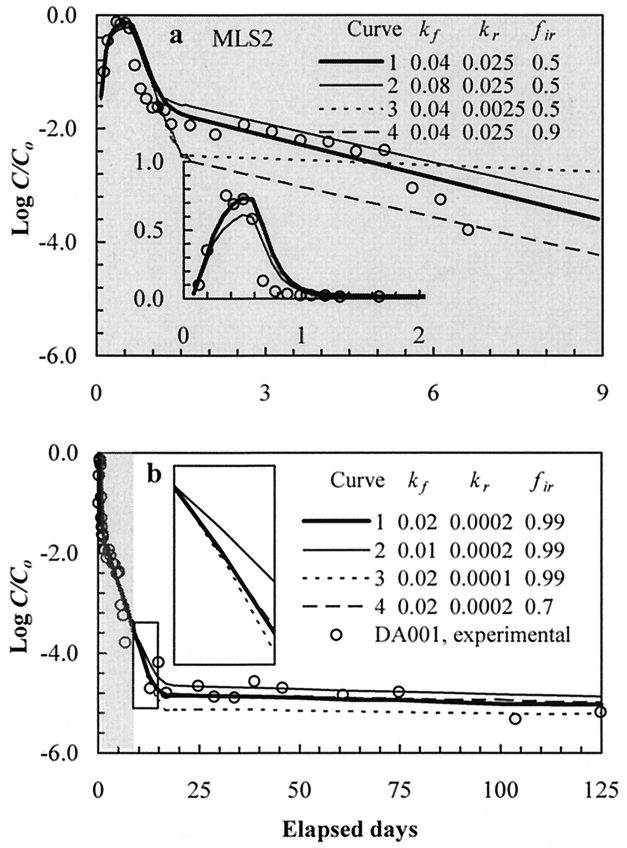

Figure 3. Sensitivity analysis under (a) forced gradient conditions and (b) natural gradient conditions. Curve 1 represents the best fit simulation.

set to zero. Simulations for bromide matched the experimental data very well; for example, efficiencies of fit ranged from 0.88 to 0.99 for the bromide simulations. MLS proximal to the injection well showed values of v that were greater than the average value (1 m d^{-1}), whereas MLS distal to the injection well showed values of v that were lower than the average value because of localized mounding of the water table associated with injection, as described in section 3.2.1.1.

The values of k_f, k_r, and f_{ir} were derived by visually fitting the particle transport model to the field bacterial breakthrough-elution data using the velocity and dispersivity determined from simulation of bromide breakthrough. The use of the same v and α_L for the bacteria and the bromide was justified by the results of moment analyses which indicated that the time for the center of the mass to arrive at each well (first moment) and the dispersivity (second moment) were similar (e.g., within 20% for the first moment and within a factor of 2 for the second moment) for the bacteria and the bromide.

The value of k_f was determined from the peak concentration of the bacterial breakthrough, since the peak concentration was sensitive to k_f but was not sensitive to k_r and f_{ir}. For example, increasing k_f significantly decreased the peak breakthrough concentration (compare curves 1 and 2 in Figure 3a inset), whereas changing k_r and f_{ir} did not change the peak breakthrough concentration (curves 1, 3, and 4 were coincident in Figure 3a inset).

Once k_f was constrained, the value of k_r was determined from the slope of the forced gradient tailing, since the slope of forced gradient tailing was sensitive to the ratio k_f/k_r. For example, increases in the ratio k_f/k_r decreased the slope of the tail (compare curves 1 and 3 in Figure 3a). The ratio of k_f/k_r ($\sim$1) determined from wells MLS 2, MLS 9, MLS 10, MLS 11, MLS 14, and MLS 17 was used for MLS 19, MLS 20, and MLS 21, since the latter wells lacked forced gradient tailing data.

For given values of k_f and k_r, the value of f_{ir} was then derived by simulating the height of the forced gradient tail, since increasing f_{ir} shifted the tail downward without changing the slope (compare curves 1 and 4 in Figure 3a). It was observed that a higher f_{ir} was associated with a lower velocity (described in section 3.2.1.4). Therefore, for wells MLS 19, MLS 20, and MLS 21, where f_{ir} values could not be constrained because of the lack of forced gradient tailing data, a value of 0.7 was used since this value was observed at wells having similar pore water velocities.

2.2.3.2. Natural gradient conditions: A velocity of 0.1 m d^{-1} was used in simulations for all MLSs under natural gradient conditions, since after the extraction wells were shut down, the regional hydraulic gradient became established and dampened the local variations in the hydraulic gradient that occurred because of injection and extraction under forced gradient conditions.

The bacterial attachment rate coefficients (k_f) under natural gradient conditions were constrained by visually fitting the steep natural gradient tailing data, since this portion of the tailing was sensitive to k_f but was not sensitive to k_r and f_{ir}. For example, increased k_f steepened the steep natural gradient tailing (curve 1 versus curve 2 in Figure 3b inset), whereas equivalent changes in k_r or f_{ir} resulted in negligible changes in steep natural gradient tailing (compare curves 1, 3, and 4 in Figure 3b inset).

Once k_f was constrained, k_r was determined by visually fitting the shallow natural gradient tailing data, since this portion of the tailing was sensitive to k_r (compare curves 1 and 3 in Figure 3b) but was not sensitive to f_{ir}. For example, variation in f_{ir} from 0.99 to 0.7 negligibly affected shallow natural gradient tailing (compare curves 1 and 4 in Figure 3b). Since the tailing concentration under natural gradient conditions was not sensitive to f_{ir}, a fixed value of 0.99 was used for all the wells. Since f_{ir} was observed to increase with decreasing velocity (described in section 3.2.1.4), the value of f_{ir} chosen to represent natural gradient conditions (v = 0.1 m d^{-1}) was increased (to 0.99) relative to the value observed under forced gradient conditions (0.7).

3. Results and Discussion

3.1. Field Data

The bacterial breakthrough-elution data from the high-permeability zone (port 9) for wells MLS 2, MLS 9, MLS 11, MLS 14, MLS 19, MLS 20, and MLS 21 (see Figure 1 for well layout) are presented in Figure 2.

Forced gradient tailing was obvious for MLS 2, MLS 9, MLS 11, and MLS 14, and the tailing concentration was about 1% of the peak concentration (Figure 2a and Figures 2c–2e insets). No forced gradient tailing was observed for MLS 19, MLS 20, and MLS 21 because of the lack of sample collection during this period (Figures 2f–2h insets).

Natural gradient tailing was observed over a 4-month period for all the wells that were monitored (Figures 2b–2h). Steep natural gradient tailing (from 9 to $\sim$20 days) showed rapidly decreasing bacterial concentrations ($\sim$2 orders of magnitude drop over 10 days), whereas shallow natural gradient tailing

Table 1. Model Parameters Determined by Simulations of Field Transport Data[a]

	Wells								
	MLS 2	MLS 10	MLS 9	MLS 11	MLS 14	MLS 17	MLS 19	MLS 20	MLS 21
				Forced Gradient					
Distance, m	0.5	1.5	1.8	1.8	2.5	3.5	4.1	4.1	5.5
Velocity, m d^{-1}	1.83	1.32	0.84	1.27	1.13	1.32	1.01	0.60	0.96
Dispersivity, m	0.12	0.05	0.13	0.03	0.08	0.05	0.30	0.29	0.15
k_f, $hour^{-1}$	0.04	0.01	0.01	0.01	0.035	0.01	0.001	0.001	0.003
k_r, $hour^{-1}$	0.025	0.01	0.01	0.01	0.02	0.01	0.001	0.001	0.003
f_{ir}	0.5	0.7	0.7	0.7	0.7	0.7	0.7	0.7	0.7
				Natural Gradient					
k_f predicted by filtration, $hour^{-1}$	0.016	NA	0.005	0.005	0.017	NA	0.0005	0.0006	0.0015
k_f fitting, $hour^{-1}$	0.02	NA	0.02	0.03	0.02	NA	0.01	0.02	0.015
k_r, $hour^{-1}$	0.0002	NA	0.00005	0.00005	0.0001	NA	0.0002	0.00025	0.0001
E, entire curve	0.97	0.92	0.89	0.92	0.77	0.60	0.83	0.90	0.94

[a]The k_f values from filtration theory under natural gradient conditions were calculated using equations (5) and (6), with the same α values (calculated using equation (7)) used for forced gradient conditions. NA stands for not available.

showed slower decreases in bacterial concentrations (~2 orders of magnitude drop over 100 days), indicating that it would take another 100 days for the aqueous bacterial concentration to drop to a few cells mL^{-1}.

The bromide tracer did not exhibit skewed breakthrough nor was tailing observed (data not shown), indicating that physical nonequilibrium transport was not significant at this site and that the observed bacterial tailing was, instead, due to detachment of previously attached bacteria. The injected bacterial pulse passed through the flow cell within 2 weeks, whereas the extended tailing of bacteria (resulting from slow detachment) lasted for months, demonstrating that bacteria can remain in the aqueous phase for prolonged periods of time (months or longer) following passage of the pulse.

The ability to monitor DA001 for several months in the field indicates that the stain did not degrade or otherwise leave the bacterial cell during this period. The ability to count low concentrations of DA001 during this period bespeaks the high resolution of ferrographic capture as a bacterial tracking technique.

3.2. Modeling Results

3.2.1. Forced gradient conditions. The transport parameters determined under forced gradient conditions are discussed in this section.

3.2.1.1. Pore water velocity *v*: The pore water velocity determined under forced gradient conditions (from simulation of the bromide data) was 1.8 m d^{-1} at MLS 2 and 0.6 m d^{-1} at MLS 20 and varied slightly (1.1 ± 0.2 m d^{-1}) among all of the other wells (Table 1 and Figure 4a). The relatively high velocity at MLS 2 was caused by localized mounding of the water table due to injection of the bacteria-bromide suspension at B2. The low velocity (0.6 m d^{-1}) at MLS 20 may be attributed to the anisotropy in hydraulic conductivity, which caused the average flow direction to skew to the east of the cell axis under forced gradient conditions [*Johnson et al*., 2001a]. Velocities showed a weak inverse relationship to distance from the injection well (Figure 4a), as would be expected from the forced gradient.

3.2.1.2. Values of k_f and k_r: Values of k_f and k_r under forced gradient conditions are listed in Table 1. The values of k_f at wells MLS 2 and MLS 14 (0.04 $hour^{-1}$ and 0.035 $hour^{-1}$, respectively) were significantly higher than the values of k_f at other wells (MLS 9, MLS 10, MLS 11, MLS 17, MLS 19, MLS 20, and MLS 21). The higher k_f value at MLS 2 may have been due to the higher velocity at this location (the expected relationship between velocity and k_f is described in section 3.2.2.1), whereas the higher k_f value at MLS 14 may be due to the migration of bacteria through the low-permeability zone between MLS 10 and MLS 14. The value of k_f at MLS 2 (0.04 $hour^{-1}$) was similar to the k_f values (0.09–0.2 $hour^{-1}$) derived from laboratory experiments examining the same bacterial strain under similar pore water velocities and an equivalent transport distance within intact cores from the Narrow Channel site. This indicates that the attachment rate coefficients determined from laboratory columns may represent the attachment rate coefficients in the field at the same scale.

Bacterial attachment and detachment rate coefficients derived from published laboratory column experiments are summarized in Table 2. The k_r values from this study were within the observed range of k_r from the literature, whereas the k_f values from this study were 1–2 orders lower than the corresponding values from the literature (Table 2). As a result, the k_f/k_r ratio from this study (1–2) was much less than the k_f/k_r ratio from the literature (10^1–10^3). The relatively low k_f values from this study may be attributed to the adhesion deficiency of the bacterial strain. It is possible that the lower values of k_f in this study may result from the larger transport distances, since k_f values may decrease as transport distances increase (see section 3.2.1.3). However, the highest k_f value observed at the shortest transport distance (50 cm, comparable to laboratory column length) in this study was still an order of magnitude lower than the k_f values from the literature (Table 2), indicating that the adhesion deficiency of the bacterial strain rather than the transport distances contributed to the relatively low values of k_f.

3.2.1.3. Rate coefficient k_f and transport distances (spatial variations in k_f): Values of k_f corresponding to forced gradient conditions decreased by a factor of ~20 over the 5-m transport distance (Figure 4b). The systematic decrease in k_f with travel distance may correspond to systematic changes in

Table 2. Summary of Bacterial Attachment and Detachment Rate Coefficients Derived From Column Experiments[a]

	Porous Media	L, cm	pH	I, mM	v, m d^{-1}	Bacteria	k_f, hour^{-1}			k_r, $\times 10^{-2}$ hour^{-1}			k_f/k_r		
							Low	High	Average	Low	High	Average	Low	High	Average
Hornberger et al. [1992]	clean quartz, 0.33–0.4 mm, 1–1.14 mm	14	6.8	0.89, 8.9	3.36	W6	0.31	5.43	2.49	1.3	7.2	4.1	8	191	75
						W8	2.15	7.58	4.53	1.5	9.0	4.0	29	263	141
McCaulou et al. [1994]	quartz, hematite, or polymer-coated quartz, 0.162 mm	21	7.3	1.1	4.0	S5	1.19	3.24	2.08	0.06	9.0	3.0	20	2,143	1,408
						S139	0.54	5.80	3.59	1.9	6.1	4.0	19	298	130
McCaulou et al. [1995]	sediments of the Ringold Formation at PNNL, 0.224 mm	30	8.0	2.8	7.8	A0500	0.58	1.69	1.08	0.2	0.6	0.4	92	691	350
Tan et al. [1994]	aquifer sand from Eastport, New York, 0.5–2 mm	30	7.0	DI, 10	4.3–17.3	*Pseudomonas* sp.	3.32	26.6	12.7	0.05	22.4	5.9	76	29,520	6,187
Hendry et al. [1997]	coarse-grained silica sand, 0.5–1 mm	11.4	7.4	2.5	0.09–0.19	*Klebsiella oxytoca*	…	…	0.10	…	…	2.0	…	…	5
Hendry et al. [1999]	coarse-grained silica sand, 0.5–1 mm	3.8–40	7.3	2.5	0.14–3.12	*Klebsiella oxytoca*	0.14	2.00	0.90	1.0	3.3	2.0	9	83	47
		3.8–40	7.3	2.5	0.12–3.2	G4PR1	0.40	2.83	2.17	0.05	0.1	0.1	400	5,660	3,310
This study	quartz, feldspars, and Fe and Al hydroxides, 0.1–0.5 mm	50–550	6	3	0.6–1.8	DA001	0.001	0.04	0.013	0.1	2.5	0.89	1	1.8	1.2

[a] L is the transport distance, I is the ionic strength, and DI stands for deionized water.

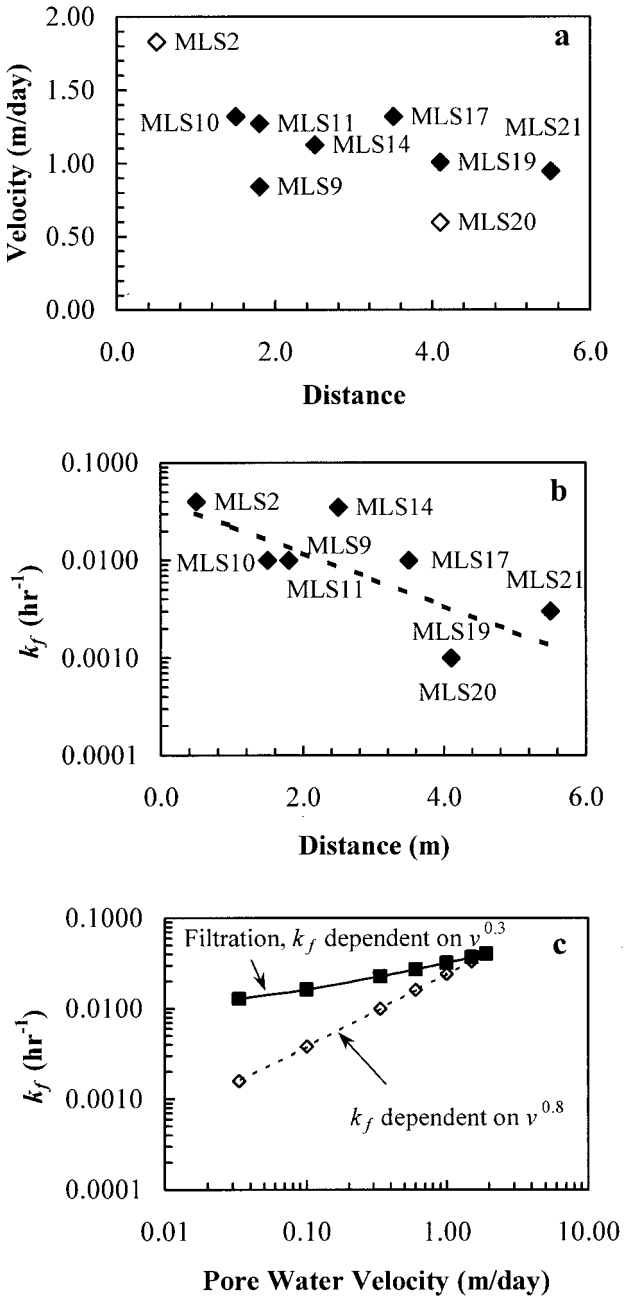

Figure 4. (a) Plots of observed velocity versus travel distance, (b) observed k_f versus travel distance, and (c) the relationship between k_f and pore water velocity. Velocities showed a weak inverse relationship to distance from the injection well. Attachment rate coefficients decreased by a factor of 20 over a transport distance of 5 m, possibly because of decreased bacterial adhesion with increased transport distance. The dashed line in Figure 4b represents the regression of the field data. The solid line in Figure 4c was calculated from filtration theory (equation (5)) using a constant α of 0.003, a grain diameter of 200 μm (d_{10}), a particle diameter of 1.1 μm, a particle density of 1.06 g cm^{-3}, and a porosity of 0.3. The dashed line in Figure 4c was calculated assuming $k_f \propto v^{0.8}$.

several parameters with distance traveled, for example, water chemistry, sediment grain size (and hydraulic conductivity), pore water velocity, and bacterial surface properties. However, physical and chemical characterizations of the site indicated

that neither grain size nor aqueous chemistry varied systematically with distance downgradient in the high-permeability zone [*Johnson et al*., 2001a; Mailloux et al., submitted manuscript, 2001]. Given that pore water velocities decreased by a factor of 3 across the flow cell (Figure 4a), decreases by a factor of 1.5–2.5 in k_f would be expected based on filtration theory (described in section 3.2.2.1 and shown in Figure 4c). The observed k_f values showed a much greater decrease (i.e., by a factor of 20) with distance across the flow cell (Figure 4b), indicating that the observed decrease in k_f may have been caused by decreased bacterial adhesion with transport distance, possibly because of alteration of the bacterial surface during transport or preferential attachment of more adhesive bacteria during transport.

Decreasing microbial attachment with increasing transport distance in the field has also been observed during transport of flagellates [*Harvey et al*., 1995] and viruses [*Schijven et al*., 1999]. In some cases, investigators have shown that the microbial collision efficiency (α) decreases with transport distance. The collision efficiency can be backed out from experimental data using filtration theory [*Harvey and Garabedian*, 1991]. However, it should be noted that estimation of the collision efficiency (α) involves division by the calculated value of the collector efficiency (η) as follows:

$$\alpha = \frac{-d \ln \mathrm{RB}}{1.5(1-\theta)\eta x}, \tag{7}$$

where RB is the relative breakthrough of bacteria [*Harvey and Garabedian*, 1991]. The collector efficiency (η) is calculated from expressions based on particle trajectory analysis (equation (6)). Hence, if the calculated value of the collector efficiency were higher or lower than its actual value, the collision efficiency would systematically increase or decrease, respectively, with transport distance. The use of the attachment rate coefficient (k_f) to quantify attachment rates avoids this potential artifact.

The observed decrease in k_f with transport distance might explain the discrepancies between the extents of bacterial transport observed in the field relative to those predicted from laboratory column experiments. For example, *Johnson et al*. [2001a] reported bacterial transport as far as 20 m within the flow cell ($C/C_0 = 5 \times 10^{-6}$), whereas model predictions based on an attachment rate coefficient estimated from 0.5-m intact cores predicted a maximum of 5 m of transport ($C/C_0 = 5 \times 10^{-6}$). The observed decrease in k_f with transport distance dictates that attachment rate coefficients determined at a scale of 0.5 m should underestimate the extent of transport at larger scales.

The observed factor of 20 decrease in k_f within 5 m of transport is comparable to differences in k_f resulting from variations in other factors such as bacterial strain, porous media, pH, ionic strength, and pore water velocity (Table 2), indicating that the influence of scale on bacterial attachment rates is as important as the aforementioned physiological and physicochemical factors. Of course, scale itself is important only in so far as it allows the effect of parameter variation to be observed, which in this case was decreasing k_f with increasing distance of transport.

3.2.1.4. Fraction of irreversibility (f_{ir}): The fraction of irreversibility (f_{ir}) was 0.5 at MLS 2 ($v = 1.8$ m d^{-1}) and 0.7 at MLS 9, MLS 10, MLS 11, MLS 14, and MLS 17 ($v \approx 1$ m d^{-1}) under forced gradient conditions, indicating that f_{ir} may have varied inversely with velocity. The possible inverse relationship between f_{ir} and pore water velocity leads to the speculation that hydrodynamic shear may have contributed to the detachment of bacteria from the sediment under forced gradient conditions. However, further study is needed to support this potential relationship.

3.2.2. Natural gradient conditions. The transport parameters determined under natural gradient conditions are discussed in this section.

3.2.2.1. Rate coefficient k_f and velocity change: As the hydraulic gradient relaxed to its natural value upon cessation of groundwater extraction at 9 days, the pore water velocity decreased by a factor of 10. As a result, the apparent values of k_f for wells MLS 2 and MLS 14 decreased by roughly a factor of 2 (Table 1). In contrast, the remaining MLSs (MLS 9, MLS 11, MLS 19, MLS 20, and MLS 21) showed increases in the apparent value of k_f by a factor of 2–20 (Table 1), despite the fact that these wells also experienced an order of magnitude decrease in velocity. The apparent value of k_f during steep natural gradient tailing was nearly equivalent for all of the MLSs (including MLS 2 and MLS 14), ranging between 0.01 and 0.03 hour^{-1} (Table 1).

The trend and magnitude of change in k_f observed in MLS 2 and MLS 14 during transition from forced to natural gradient conditions (factor of 2 decrease) is in accordance with filtration theory. Assuming independence of the attachment efficiency (α) on pore water velocity, filtration theory (equation (5)) along with the particle trajectory equations of *Rajagopalan and Tien* [1976] predicts that k_f should vary directly with pore water velocity (to the power of 0.3) under our experimental conditions (diffusion dominating as the mechanism of collision) (Figure 4c). Increasing k_f with pore water velocity has been observed in other colloidal transport experiments. For example, at low to moderate pore water velocities (i.e., 0.1–50 m d^{-1}), *Tan et al*. [1994] and *Hendry et al*. [1999] found that the values of k_f for bacteria were dependent upon velocity to the power of ~0.8, and *Kretzschmar et al*. [1997] found that the values of k_f for latex and humic-coated hematite colloids increased with velocity to the power of 0.18–0.31.

For MLS 9, MLS 11, MLS 19, MLS 20, and MLS 21 the observed increases in apparent k_f (by a factor of 2–20) upon relaxation to natural gradient conditions were opposite in trend and of much greater magnitude relative to what was predicted based on filtration theory (Table 1 and Figure 4c), since filtration theory predicted a factor of 2 decrease in k_f. Furthermore, the apparent k_f values attained during steep natural gradient tailing were nearly equivalent for all of the MLSs. These results indicate that pore water velocity may not have controlled bacterial attachment to the sediment during steep natural gradient tailing and, more accurately, that filtration may not have been the dominant mechanism of loss of bacteria from the aqueous phase under natural gradient conditions.

3.2.2.2. Rate coefficient k_f and predation: An additional potential mechanism of bacterial loss from the aqueous phase is predation of the bacteria, for example, by protozoa. Protozoa (flagellates) were observed in all of the MLSs (Figure 2). There were 7–10 days of lag between the peak of the flagellate bloom and the peak of the injected bacterial pulse. The flagellate bloom lasted ~10 days for all of the wells (Figure 2).

The onset of steep natural gradient tailing (increased bacterial removal, k_f, for most of the wells) coincided with the appearance of flagellates in all of the MLSs (Figure 2), whereas a decreased slope to shallow natural gradient tailing

(indicating a decreased rate of bacterial removal from aqueous phase) coincided with cessation of the flagellate blooms (Figure 2). This result suggests that predation, rather than filtration, controlled the removal of bacteria from the aqueous phase during steep natural gradient tailing.

Close examination of MLS 2 data revealed that the bacterial concentration decreased rapidly at 5 days (Figure 2a), coincident with the onset of the flagellate bloom, despite the fact that the velocity had not yet decreased (groundwater extraction did not cease until 9 days into the experiment). Furthermore, the slope of the tail between 5 and 15 days remained relatively constant despite the order of magnitude decrease in velocity after 9 days, further supporting the hypothesis that predation rather than velocity controlled the loss of bacteria from the aqueous phase during this period.

Simulations of bacterial tailing concentrations based on kinetic constants extrapolated from forced gradient conditions to natural gradient conditions based on filtration theory (Table 1) are shown as dashed curves (Figures 2b–2h). The difference between these simulated tails and the best fit simulations (solid curves in Figures 2b–2h) during the period of 9–20 days was used to estimate the number of bacteria grazed during this period. The ratio of grazed bacteria to flagellates during this period ranged from 2 to 2500 (corresponding to a predation rate of 0.01–9.5 bacteria flagellate^{-1} hour^{-1}) among the different MLSs. Predation rates from the literature for similar sized flagellates (3–4 μm in diameter) range from 0.04 to 14 bacteria flagellate^{-1} hour^{-1} [*Sherr et al*., 1988; *Holen and Boraas*, 1991; *Kinner et al*., 1998], indicating that the observed loss of bacteria can be reasonably ascribed to flagellates, although loss due to other protists (e.g., ciliates and amoebae) and bacteriophage may have also occurred.

The inflection marking the transition between steep and shallow natural gradient tailing occurred because of depletion of aqueous phase bacteria, since values of k_f and k_r were kept constant (for a given MLS) during the entire natural gradient tailing. The apparent attachment rate coefficients k_f may have decreased after predation ceased (beginning of shallow natural gradient tailing). However, because of the covariations of k_f and k_r during shallow natural gradient tailing it was not possible to determine unique values of k_f and k_r during this period.

3.2.2.3. Rate coefficient k_r and velocity change: The values of k_r decreased by more than an order of magnitude as the velocity decreased by a factor of 10 (Table 1). The k_r values may have been underestimated, however, since grazing of attached bacteria may have lowered the values of S and S_r. Since predation operated during natural gradient tailing, it was not possible to distinguish the effects of predation from the potential effects of decreased velocity (e.g., decreased hydrodynamic shear) or residence time (e.g., active adhesion processes) on detachment during the transition from forced to natural gradient conditions.

3.2.2.4. Rate coefficient k_r and rainfall: Simulations of shallow natural gradient tailing showed flat tails, whereas experimental data showed increased bacterial concentrations at ~40 days for all of the MLSs (Figures 2b–2h). This concentration increase was not caused by the analytical error of the ferrographic tracking technique because the variations in observed concentrations were much greater than the analytical error of the tracking method (typically <20%). The concentration increase at 40 days coincided with the first series of rainfall events at 35–45 days after the field injection, possibly

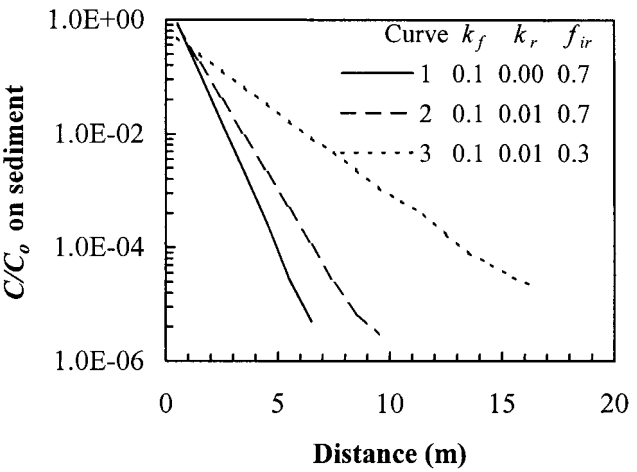

Figure 5. Simulated bacterial concentration (C/C_0) on sediment phase after 125 days of injection (v = 1.0 m d^{-1}, α_L = 0.1 m, and 12-hour input). Simulations with detachment (curves 2 and 3) showed significant downgradient movement of the attached population relative to the case lacking detachment (curve 1).

indicating an increase in the bacterial detachment rate in response to either a decreased ionic strength or increased pore water velocity (increased hydrodynamic shear) in response to recharge. Data collected using Multi-Parameter Troll (In Situ, Inc.) between 40 and 125 days following the injection indicated that conductivity and pH remained relatively constant (e.g., conductivity ranged from 265 to 275 microSiemens cm^{-1}, and pH ranged from 5 to 6 during this period). Hence the increased pore water velocity, rather than the change in ionic strength, in response to rainfall may have contributed to the observed increase in bacterial detachment. Rainfall events that occurred after 70 days showed no significant increases in tail concentrations. However, this may not indicate a lack of increased detachment in response to recharge since increased aqueous bacterial concentrations may have been missed because of infrequent sampling between 70 and 120 days. Alternatively, there may have been an insignificant detachment response because of a low or irreversibly attached bacterial population after 70 days.

3.2.3. Travel distance achieved with and without detachment. Simulations were performed to examine the transport distances achieved with and without detachment after 125 days of injection, using attachment and detachment rate coefficients similar to those obtained in this field study (e.g., k_f = 0.1 hour^{-1} and k_r = 0.01 hour^{-1}). Simulations without detachment showed steep exponentially decreasing concentrations in the sediment with distance from the source (curve 1 in Figure 5). Simulations with 30% reversible attachment (f_{ir} = 0.7 and k_r = 0.01 hour^{-1}) showed significant downgradient movement of the attached population (curve 2 in Figure 5) relative to the case lacking detachment. This downgradient movement of the attached population became even more significant as the reversibility increased to 70% (f_{ir} = 0.3, curve 3 in Figure 5). For a given C/C_0 of 10^{-5} on the sediment phase, bacterial transport distance achieved with k_r = 0.01 hour^{-1} and f_{ir} = 0.3 was 18 m, nearly 3 times the distance achieved in absence of detachment (Figure 5). The above modeling results clearly demonstrated that detachment could significantly increase the

transport distances over long time. However, a variety of bacterial, sediment surface, and water chemistries need to be examined to determine the relative magnitudes of attachment and detachment rates, as well as the reversibility of attachment, under various conditions.

4. Summary and Conclusions

Extended tailing of bacteria (DA001) following breakthrough at the Narrow Channel Focus Area was observed for 4 months, demonstrating that low concentrations of bacteria were present in the aqueous phase for prolonged times (several months or longer) after the "source" (e.g., the injected pulse) had passed.

Bacterial attachment and detachment kinetics associated with breakthrough and extended tailing were determined by fitting a 1-D transport model to the field breakthrough-tailing data. The dependence of attachment rate coefficients on transport distances was examined by comparing the attachment rate coefficients at different MLSs (different transport distances). Attachment rate coefficients (k_f) under forced gradient conditions decreased as travel distance increased, possibly because of decreased bacterial adhesion with increased transport distance. Hence the use of kinetic constants derived from laboratory column experiments may underpredict the extent of bacterial transport at larger scales (e.g., field scales).

The effects of velocity change on the apparent attachment and detachment rates were examined at two velocities differing by an order of magnitude. Apparent bacterial attachment rate coefficients did not decrease with velocity as expected from filtration theory but, instead, increased greatly for most of the wells. The coincidence of the increase in apparent attachment rate coefficient with the occurrence of flagellate blooms suggested that the loss of bacteria from the aqueous phase during this stage of tailing (9–20 days) was not governed by filtration but rather by predation. Detachment rate coefficients decreased significantly as velocity decreased, but possible effects of decreased hydrodynamic shear could not be separated from potential effects of predation and residence time.

Simulations were performed to examine the transport distances achieved with and without detachment using attachment and detachment rate coefficients similar to those obtained in this field study. Simulations that included detachment showed that transport distances of bacteria may significantly increase because of detachment under the conditions examined.

Acknowledgments. This work was funded by U.S. Department of Energy (DOE), Natural and Accelerated Bioremediation Research Program (NABIR)—Acceleration Element (grants DE-FG03-99ER62820/A000 and DE-FG02-99ER62821). The authors would also like to acknowledge the leadership of Frank Wobber, the Program Manager for the Acceleration Element of NABIR. Access to the field site was granted by The Nature Conservancy, Virginia Coast Reserve.

References

Ahlstrom, S. W., H. P. Foote, C. Arnett, C. R. Cole, and R. J. Serne, Multicomponent mass transport model: Theory and numerical implementation (discrete parcel random walk version), *Tech. Rep. BNWL-2127*, Battelle Pac. Northwest Lab., Richland, Wash., 1977.

Albinger, O., B. K. Biesemeyer, R. G. Arnold, and B. E. Logan, Effect of bacterial heterogeneity on adhesion to uniform collectors by monoclonal populations, *FEMS Microbiol. Lett*., *124*, 321–326, 1994.

Baygents, J. C., J. R. Glynn Jr., O. Albinger, B. K. Biesemeyer, K. L. Ogden, and R. G. Arnold, Variation of surface charge density in monoclonal bacterial populations: Implications for transport through porous media, *Environ. Sci. Technol*., *32*, 1596–1603, 1998.

Bolster, C. H., A. L. Mills, G. M. Hornberger, and J. S. Herman, Spatial distribution of deposited bacteria following miscible displacement experiments in intact cores, *Water Resour. Res*., *35*, 1797–1807, 1999.

Bolster, C. H., A. L. Mills, G. Hornberger, and J. Herman, Effect of intra-population variability on the long-distance transport of bacteria, *Ground Water*, *38*, 370–375, 2000.

DeBorde, D. C., W. W. Woessner, Q. T. Kiley, and P. Ball, Rapid transport of viruses in a floodplain aquifer, *Water Resour. Res*., *33*, 2229–2238, 1999.

DeFlaun, M. F., A. Tanzer, A. McAteer, B. Marshall, and S. Levy, Development of an adhesion assay and characterization of an adhesion-deficient mutant of Pseudomonas-Fluorescens, *Appl. Environ. Microbiol*., *56*, 112–119, 1990.

DeFlaun, M. F., M. E. Fuller, W. P. Johnson, P. Zhang, B. J. Mailloux, T. C. Onstott, W. Holben, D. Balkwill, and D. White, Comparison of innovative methods for monitoring bacterial transport, *J. Microbiol. Methods*, in press, 2001.

Fontes, D. E., A. L. Mills, G. M. Hornberger, and J. S. Herman, Physical and chemical factors influencing transport of microorganisms through porous media, *Appl. Environ. Microbiol*., *57*, 2473–2481, 1991.

Fuller, M. E., S. Streger, R. Rothmel, B. Mailloux, T. C. Onstott, J. Fredrickson, D. Balkwill, and M. F. DeFlaun, Development of a vital fluorescent staining method for monitoring bacterial transport in subsurface environments, *Appl. Environ. Microbiol*., *66*, 4486–4496, 2000.

Fuller, M. E., B. Mailloux, P. Zhang, S. Vainberg, W. P. Johnson, T. C. Onstott, and M. F. DeFlaun, Evaluation of CFDA/SE-staining coupled with multiple detection methods during a field-scale bacterial transport experiment, *FEMS Microbiol. Ecol*., in press, 2001.

Glynn, J. R., Jr., B. M. Belongia, R. G. Arnold, K. L. Ogden, and J. C. Baygents, Capillary electrophoresis measurements of electrophoretic mobility for colloidal particles of biological interest, *Appl. Environ. Microbiol*., *64*, 2572–2577, 1998.

Harter, T. H., S. Wagner, and E. R. Atwill, Colloid transport and filtration of *Cryptosporidium parvum* in sandy soils and aquifer sediments, *Environ. Sci. Technol*., *34*, 62–70, 2000.

Harvey, R. W., and S. P. Garabedian, Use of colloid filtration theory in modeling movement of bacteria through a contaminated sandy aquifer, *Environ. Sci. Technol*., *25*, 178–185, 1991.

Harvey, R. W., N. E. Kinner, A. Bunn, D. MacDonald, and D. W. Metge, Transport behavior of groundwater protozoa and protozoan-sized microspheres in sandy aquifer sediments, *Appl. Environ. Microbiol*., *61*, 209–217, 1995.

Hendry, M. J., J. R. Lawrence, and P. Maloszewski, The role of sorption in the transport of *Klebsiella oxytoca* through saturated silica sand, *Ground Water*, *35*, 574–584, 1997.

Hendry, M. J., J. R. Lawrence, and P. Maloszewski, Effects of velocity on the transport of two bacteria through saturated sand, *Ground Water*, *37*, 103–112, 1999.

Holen, D. A., and M. E. Boraas, The feeding behavior of *Spumella sp*. as a function of particle size: Implications for bacterial size in pelagic systems, *Hydrobiologia*, *220*, 73–88, 1991.

Hornberger, G. M., A. L. Mills, and J. S. Herman, Bacterial transport in porous media: Evaluation of a model using laboratory observations, *Water Resour. Res*., *28*, 915–938, 1992.

Hubbard, S. S., J. Chen, J. Peterson, E. Majer, Y. Rubin, K. Williams, and D. Swift, Hydrogeological characterization of the South Oyster Bacterial Transport Site using geophysical data, *Water Resour. Res*., *37*, 2431–2456, 2001.

Johnson, W. P., K. A. Blue, B. E. Logan, and R. G. Arnold, Modeling bacterial detachment during transport through porous media as a residence-time-dependent process, *Water Resour. Res*., *31*, 2649–2658, 1995.

Johnson, W. P., et al., Ferrographic tracking of bacterial transport in the field at the Narrow Channel Focus Area, Oyster, VA, *Environ. Sci. Technol*., *35*, 182–191, 2001a.

Johnson, W. P., P. Zhang, P. M. Gardner, M. E. Fuller, and M. F. DeFlaun, Indication of detachment of indigenous bacteria from aquifer sediment in response to bacterial injection experiments, *Appl. Environ. Microbiol*., in press, 2001b.

Kinner, N. E., R. W. Harvey, K. Blakeslee, G. Novarino, and L. D.

Meeker, Size-selective predation on groundwater bacteria by nanoflagellates in an organic-contaminated aquifer, *Appl. Environ. Microbiol*., *64*, 618–625, 1998.

Kinzelbach, W., and G. Uffink, The random walk method and extensions in groundwater modeling, in *Transport Processes in Porous Media*, edited by J. Bear and M. Y. Corapcioglu, pp. 761–787, Kluwer Acad., Norwell, Mass., 1991.

Kretzschmar, R., K. Barmettler, D. Grolimund, Y. Yan, M. Borkovec, and H. Sticher, Experimental determination of colloid deposition rates and collision efficiencies in natural porous media, *Water Resour. Res*., *33*, 1129–1137, 1997.

Lindqvist, R., J. S. Cho, and C. G. Enfield, A kinetic model for cell density dependent bacterial transport in porous media, *Water Resour. Res*., *30*, 3291–3299, 1994.

Logan, B. E., D. G. Jewett, R. G. Arnold, E. J. Bouwer, and C. R. O'Melia, Clarification of cleanbed filtration models, *J. Environ. Eng*., *121*, 869–873, 1995.

Martin, M. J., B. E. Logan, W. P. Johnson, D. G. Jewett, and R. G. Arnold, Scaling bacterial filtration rates in different sized porous media, *J. Environ. Eng*., *122*, 407–415, 1996.

McCaulou, D. R., R. C. Bales, and J. F. McCarthy, Use of short-pulse experiments to study bacteria transport through porous media, *J. Contam. Hydrol*., *15*, 1–14, 1994.

McCaulou, D. R., R. C. Bales, and R. G. Arnold, Effect of temperature-controlled motility on transport of bacteria and microspheres through saturated sediment, *Water Resour. Res*., *31*, 271–280, 1995.

Murphy, E. M., and T. R. Ginn, Modeling microbial processes in porous media, *Hydrogeol. J*., *8*, 142–158, 2000.

Peterson, T. C., and R. C. Ward, Development of a bacterial transport model for coarse soils, *Water Resour. Bull*., *25*, 349–357, 1989.

Poeter, E. P., and M. C. Hill, Documentation of UCODE, a computer code for universal inverse modeling, *U.S. Geol. Surv. Water Resour. Invest. Rep*., *98-4080*, 116 pp., 1998.

Prickett, T. A., T. C. Naymik, and C. G. Lonnquist, A random-walk solute transport model for selected groundwater quality evaluations, *Tech. Rep. Bull*., *65*, 103 pp., Ill. State Water Surv., Champaign, 1981.

Rajagopalan, R., and C. Tien, Trajectory analysis of deep-bed filtration with the sphere-in-a-cell porous media model, *AIChE J*., *22*, 523–533, 1976.

Rajagopalan, R., C. Tien, R. Pfeffer, and G. Tardos, Letter to the editor, *AIChE J*., *28*, 871–872, 1982.

Ryan, J. N., and M. Elimelech, Colloid mobilization and transport in groundwater, *Colloids Surf. A*, *107*, 1–56, 1996.

Ryan, J. N., M. Elimelech, R. A. Ard, R. W. Harvey, and P. R. Johnson, Bacteriophage PRD1 and silica colloid transport in an iron oxide-coated sand aquifer, *Environ. Sci. Technol*., *33*, 63–73, 1999.

Scheibe, T. D., Y.-J. Chien, and J. S. Radtke, Use of quantitative models to design microbial transport experiments in a sandy aquifer, *Ground Water*, *39*, 210–222, 2001.

Schijven, J. F., W. Hoogenboezem, S. M. Hassanizadeh, and J. H. Peters, Modeling removal of bacteriophages MS2 and PRD1 by dune recharge at Castricum, Netherlands, *Water Resour. Res*., *35*, 1101–1111, 1999.

Scholl, M. A., and R. W. Harvey, Laboratory investigations on the role of sediment surface and groundwater chemistry on the transport of bacteria through a contaminated sandy aquifer, *Environ. Sci. Technol*., *26*, 1410–1417, 1992.

Sherr, B. F., E. B. Sherr, and F. Rassoulzadegan, Rates of digestion of bacteria by marine phagotrophic protozoa: Temperature dependence, *Appl. Environ. Microbiol*., *54*, 1091–1095, 1988.

Simoni, S. F., H. Harms, T. N. P. Bosma, and A. J. B. Zehnder, Population heterogeneity affects transport of bacteria through sand columns at low flow rates, *Environ. Sci. Technol*., *32*, 2100–2105, 1998.

Smith, M. S., G. W. Thomas, R. E. White, and D. Ritonga, Transport of *Escherichia coli* through intact and disturbed soil columns, *J. Environ. Qual*., *14*, 87–91, 1985.

Tan, Y., J. T. Gannon, P. Baveye, and M. Alexander, Transport of bacteria in an aquifer sand: Experiments and model simulations, *Water Resour. Res*., *30*, 3243–3252, 1994.

Tien, C., *Granular Filtration of Aerosols and Hydrosols*, vol. 1, edited by B. Haward, Butterworth-Heinemann, Woburn, Mass., 1989.

Tompson, A. F. B., and L. W. Gelhar, Numerical simulation of solute transport in three-dimensional, randomly heterogeneous porous media, *Water Resour. Res*., *26*, 2514–2562, 1990.

Toride, N., F. J. Leij, and M. T. van Genuchten, The CXTFIT code for estimating transport parameters from laboratory or field tracer experiments, Version 2.1, *Res. Rep. 137*, U.S. Salinity Lab., Agric. Res. Serv., U.S. Dep. Agric., Riverside, Calif., 1995.

Wollum, A. G., and D. K. Cassel, Transport of microorganisms in sand columns, *Soil. Sci. Soc. Am. J*., *42*, 72–76, 1978.

K.-Y. Choi and F. C. Dobbs, Department of Ocean, Earth and Atmospheric Sciences, Old Dominion University, Norfolk, VA 23529, USA.

W. P. Johnson, Department of Geology and Geophysics, University of Utah, Salt Lake City, UT 84112, USA. (wjohnson@mines.utah.edu)

B. J. Mailloux, Department of Geosciences, Princeton University, Princeton, NJ 08544, USA.

T. D. Scheibe, Pacific Northwest National Laboratories, Richland, WA 99352, USA.

P. Zhang, Department of Earth and Environmental Science, New Mexico Institute of Mining and Technology, Socorro, NM 87801, USA.

(Received December 18, 2000; revised May 16, 2001;
accepted May 31, 2001.)